Forced solitary waves and fronts past submerged obstacles

B. J. Binder[a] and J.-M. Vanden-Broeck[b]
School of Mathematics, University of East Anglia, Norwich NR4 7TJ, United Kingdom

F. Dias[c]
Centre de Mathématiques et de Leurs Applications, Ecole Normale Supérieure de Cachan, Cachan, France

(Received 10 February 2005; accepted 14 June 2005; published online 21 October 2005)

Herein, an efficient numerical method is presented to describe the flow of a liquid in an open channel with various types of bottom configurations. The method is developed for steady two-dimensional potential free surface flows. The resulting nonlinear problem is solved numerically by boundary integral equation methods. In addition weakly nonlinear solutions are derived. New solutions which complement those of Dias and Vanden-Broeck [J. Fluid Mech. **59**, 93–102 (2004)] are presented. Furthermore some solutions for channel flows past dips in the bottom are discussed. © *2005 American Institute of Physics*. [DOI: 10.1063/1.1992407]

Free solitary waves and fronts have been studied extensively from both an analytical and a numerical point of view. In contrast, forced solitary waves and fronts, which occur more often in nature or in experiments, have been less studied. The paper studies steady nonlinear two-dimensional open-channel flow past submerged obstructions. With several obstructions, a lot of configurations are possible. New configurations are discovered through a weakly nonlinear analysis of the problem and confirmed by numerical results.

I. INTRODUCTION

Whereas the study of solitary waves and fronts has been quite active for the past decades, the study of forced solitary waves and fronts has been much less extensive. Such forced waves occur naturally in many physical systems. Here the emphasis is on steady nonlinear two-dimensional free surface flows past submerged objects. Such flows have been studied for example by Watters and Street (1964), Forbes (1981, 1988), Dias and Vanden-Broeck (1989), and Shen (1995). The monograph by Baines (1995) provides a good description of analytical and experimental results on forced free-surface waves, even though it is primarily devoted to forced waves in stratified flows. The fluid is assumed to be inviscid and incompressible and the flow to be irrotational. A typical flow configuration with two submerged objects is shown in Fig. 1(a). Cartesian coordinates (x^*, y^*) with the x^* axis on the horizontal bottom are defined. As $x^* \to \infty$, the flow approaches a uniform stream with constant velocity U and constant depth H [see Fig. 1(a)]. We define the Froude number

$$F = \frac{U}{(gH)^{1/2}}, \tag{1}$$

where g is the acceleration due to gravity. As $x^* \to -\infty$ the flow can be uniform or possess a train of waves. When it is uniform, the Froude number

$$F^* = \frac{U^*}{(gH^*)^{1/2}} \tag{2}$$

is also introduced, where U^* and H^* are the uniform velocity and uniform depth as $x^* \to -\infty$.

In the case of one submerged obstacle, four basic flows have been identified. The first basic flow is supercritical with $F = F^* > 1$. The second is subcritical with $F < 1$ and a train of waves as $x^* \to -\infty$ (the direction of flow needs then to be reversed to satisfy the radiation condition). The third is a hydraulic jump with $F > 1$ and $F^* < 1$. The fourth is called a generalized hydraulic jump and is characterized by $F > 1$ and a train of waves as $x^* \to -\infty$. The first three basic flows are classical and the fourth was first calculated by Dias and Vanden-Broeck (2002). Generalized hydraulic jumps for flows past one submerged object lack physical meaning because the waves on the free surface do not satisfy the radiation condition. However Dias and Vanden-Broeck (2004), guided by experimental results and by the work of Pratt (1984), showed that these generalized hydraulic jumps can be used to describe locally the flow past one obstacle when a second obstacle is placed in the flow. More precisely Dias and Vanden-Broeck (2004) constructed a "hybrid" flow past two submerged obstacles which can be viewed as the superposition of two basic flows past a single obstacle (a subcritical one and a generalized hydraulic jump). The purpose of this paper is to examine further flows with two obstacles in order to classify the possible solutions. Both numerical techniques based on boundary integral equation methods and weakly nonlinear theories are used. Boundary integral equation methods have been used by many previous investigators to compute two-dimensional free-surface flows as in the

[a]Electronic mail: b.binder@uea.ac.uk
[b]Electronic mail: J.Vanden-broeck@uea.ac.uk
[c]Electronic mail: dias@cmla.ens-cachan.fr

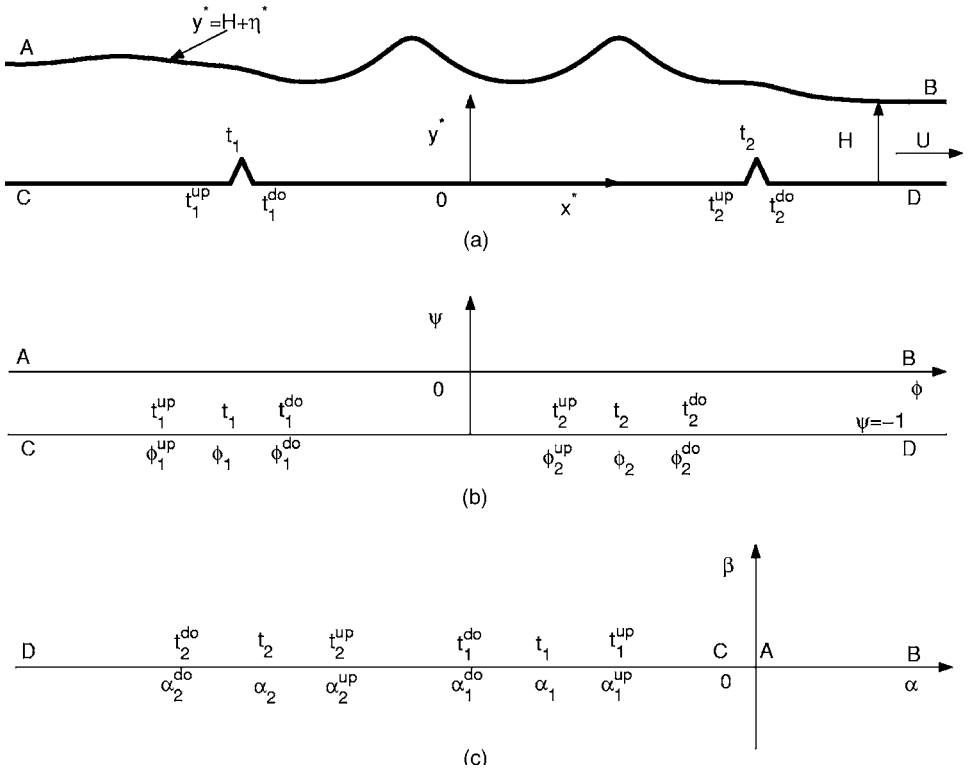

FIG. 1. (a) Sketch of the flow in physical coordinates (x^*, y^*). (b) Sketch of the flow in the plane of the complex potential (f plane). (c) Sketch of the flow in the lower half-plane (ζ plane). Various points have been labeled along the free surface and the bottom.

present paper, but also to compute two-dimensional axisymmetric and three-dimensional free-surface flows [see Dias and Bridges (2005) for a recent review]. They lead to very accurate solutions because they only require mesh points on the boundaries. In the following, classical solutions are recovered and new "hybrid" flows are discovered.

II. FORMULATION AND NUMERICAL PROCEDURE

We consider steady two-dimensional potential free surface flows past two submerged obstacles at the bottom of a channel [see Fig. 1(a)]. The results presented in this paper are qualitatively independent of the shape of the obstacles. For simplicity, triangular obstacles with corners $t_1^{\rm up}$, t_1, $t_1^{\rm do}$, $t_2^{\rm up}$, t_2 and $t_2^{\rm do}$ are chosen. Here "do" and "up" refer to downstream and upstream, respectively. Cartesian coordinates (x^*, y^*) with the x^* axis along the bottom and the y^* axis directed vertically upwards are introduced. The acceleration due to gravity g is acting in the negative y^* direction. The flow is assumed to be steady and characterized by a uniform stream with constant velocity U and constant depth H as $x^* \to \infty$. The reader interested in unsteady flows past disturbances is referred to Grimshaw and Smyth (1986). The equation of the free surface can be written as $y^* = H + \eta^*(x^*)$. We define dimensionless variables by taking H as the reference length and U as the reference velocity. Thus we define the dimensionless coordinates $(x, y) = (x^*, y^*)/H$. The free surface is then described by $y = 1 + \eta^*/H$.

The two triangles are assumed to be isosceles triangles with right angles at their apexes $x_i = x_i^*/H$, heights $h_i = h_i^*/H$, and supports $[x_i - h_i, x_i + h_i]$, $i = 1, 2$. The dynamic boundary condition on the free surface gives

$$\frac{1}{2}(u^2 + v^2) + \frac{1}{F^2} y = \frac{1}{2} + \frac{1}{F^2}, \tag{3}$$

where F is the Froude number defined by Eq. (1). Here u and v are the horizontal and vertical components of the velocity.

Next we define the potential function ϕ, the stream function ψ, and the complex potential $f = \phi + i\psi$. Without loss of generality we choose $\psi = 0$ on the free surface and $\phi = 0$ at the point $x = 0$ on the free surface. It follows that $\psi = -1$ on the bottom. The flow domain in the complex f plane is the strip $-1 < \psi < 0$ [see Fig. 1(b)]. The corners of the triangles are on the streamline $\psi = -1$. The values of ϕ at the apexes are denoted by ϕ_i, $i = 1, 2$, and those at the upstream and downstream corners of the two triangles by $\phi_i^{\rm up}$ and $\phi_i^{\rm do}$, $i = 1, 2$.

The strip $-1 < \psi < 0$ is mapped onto the lower half ζ plane by the transformation

$$\zeta = \alpha + i\beta = e^{\pi f}. \tag{4}$$

The flow configuration in the ζ plane is shown in Fig. 1(c).

The function $\tau - i\theta$ is defined by

$$u - iv = e^{\tau - i\theta} \tag{5}$$

and we apply Cauchy integral equation formula to the function $\tau - i\theta$ in the ζ plane with a contour consisting of the α axis and a semicircle of arbitrary large radius in the lower half plane. Since $\tau - i\theta \to 0$ as $|\zeta| \to \infty$, there is no contribu-

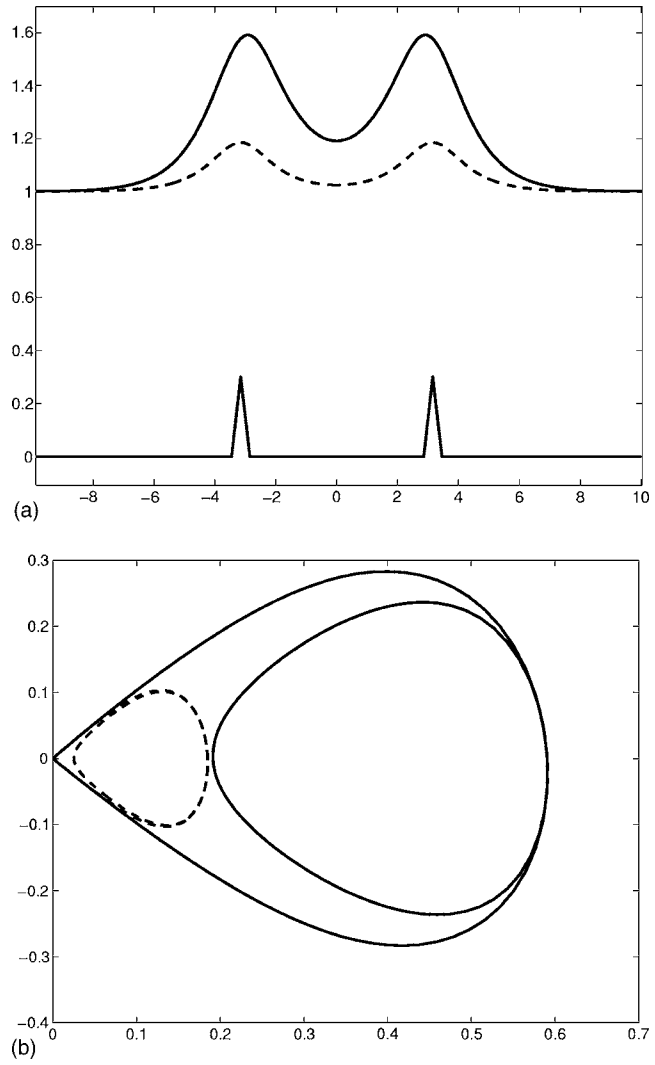

FIG. 2. Supercritical flows, for $F=1.30$, $h_1=h_2=0.30$, and $x_d=x_2-x_1=6.32$. (a) Fully nonlinear free surface profiles. The solid curve has maximum elevation 0.59 at $x=\pm 2.89$ and elevation 0.19 at $x=0$. The broken curve has maximum elevation 0.18 at $x=\pm 3.16$ and elevation 0.03 at $x=0$. The maximum elevations do not occur exactly above the top of the obstacles. (b) Values of $dy/dx=\tan(\theta)$ vs $y-1=\eta$, showing the fully nonlinear phase trajectories for (a).

tion from the half circle and we obtain (after taking the real part)

$$\tilde{\tau}(\alpha)=\frac{1}{\pi}\int_{-\infty}^{\infty}\frac{\tilde{\theta}(\alpha_0)}{\alpha_0-\alpha}d\alpha_0, \tag{6}$$

where $\tilde{\tau}(\alpha)$ and $\tilde{\theta}(\alpha)$ are the values of τ and θ on the α axis. The integral in Eq. (6) is a Cauchy principal value.

We assume that $\alpha>0$ (i.e., that α corresponds to points on the free surface). The kinematic boundary condition on the bottom of the channel implies $\tilde{\theta}(\alpha_0)=\pi/4$ for $\alpha_1<\alpha_0<\alpha_1^{\mathrm{up}}$ and for $\alpha_2<\alpha_0<\alpha_2^{\mathrm{up}}$, $\tilde{\theta}(\alpha_0)=-\pi/4$ for $\alpha_1^{\mathrm{do}}<\alpha_0<\alpha_1$ and $\alpha_2^{\mathrm{do}}<\alpha_0<\alpha_2$ and $\tilde{\theta}(\alpha_0)=0$ otherwise. Substituting these values in Eq. (6) gives

$$\tilde{\tau}(\alpha)=-\frac{1}{4}\ln\frac{(\alpha_1-\alpha)^2}{(\alpha_1^{\mathrm{up}}-\alpha)(\alpha_1^{\mathrm{do}}-\alpha)}-\frac{1}{4}\ln\frac{(\alpha_2-\alpha)^2}{(\alpha_2^{\mathrm{up}}-\alpha)(\alpha_2^{\mathrm{do}}-\alpha)}+\int_0^{\infty}\frac{\tilde{\theta}(\alpha)}{\alpha_0-\alpha}d\alpha_0. \tag{7}$$

We rewrite Eq. (7) in terms of ϕ by using the change of variables

$$\alpha=e^{\pi\phi},\quad \alpha_0=e^{\pi\phi_0}. \tag{8}$$

This gives

$$\tau(\phi)=-\frac{1}{4}\ln\frac{(e^{\pi\phi_1}+e^{\pi\phi})^2}{(e^{\pi\phi_1^{\mathrm{up}}}+e^{\pi\phi})(e^{\pi\phi_1^{\mathrm{do}}}+e^{\pi\phi})}-\frac{1}{4}\ln\frac{(e^{\pi\phi_2}+e^{\pi\phi})^2}{(e^{\pi\phi_2^{\mathrm{up}}}+e^{\pi\phi})(e^{\pi\phi_2^{\mathrm{do}}}+e^{\pi\phi})}+\int_{-\infty}^{\infty}\frac{\theta(\phi_0)e^{\pi\phi_0}}{e^{\pi\phi_0}-e^{\pi\phi}}d\phi_0. \tag{9}$$

Here $\tau(\phi)=\tilde{\tau}(e^{\pi\phi})$ and $\theta(\phi)=\tilde{\theta}(e^{\pi\phi})$.

Differentiating Eq. (3) with respect to ϕ and using Eq. (5) and the identity

$$x_\phi+iy_\phi=\frac{1}{u-iv}=e^{-\tau+i\theta} \tag{10}$$

yields

$$e^{2\tau(\phi)}\frac{\partial\tau(\phi)}{\partial\phi}+\frac{1}{F^2}e^{-\tau(\phi)}\sin\theta(\phi)=0. \tag{11}$$

Equations (9) and (11) define a nonlinear system of integro-differential equations for $\tau(\phi)$ and $\theta(\phi)$ on the free surface. Once this system has been solved numerically, the shape of the free surface is obtained in a parametric form by integrating Eq. (10). This gives

$$x(\phi)=\int_0^{\phi}e^{-\tau(\phi_0)}\cos\theta(\phi_0)d\phi_0\quad\text{for}\ -\infty<\phi<\infty, \tag{12}$$

$$y(\phi)=1+\int_{\infty}^{\phi}e^{-\tau(\phi_0)}\sin\theta(\phi_0)d\phi_0\quad\text{for}\ -\infty<\phi<\infty. \tag{13}$$

A. Numerical scheme

Equations (9) and (11) are solved numerically. Equally spaced mesh points in the potential function ϕ are introduced:

$$\phi_I=[-(N-1)/2+(I-1)]\Delta,\quad I=1,\ldots,N. \tag{14}$$

Here $\Delta>0$ is the mesh size. The corresponding unknowns are

$$\theta_I=\theta(\phi_I),\quad I=1,\ldots,N. \tag{15}$$

The function τ is evaluated at the midpoints

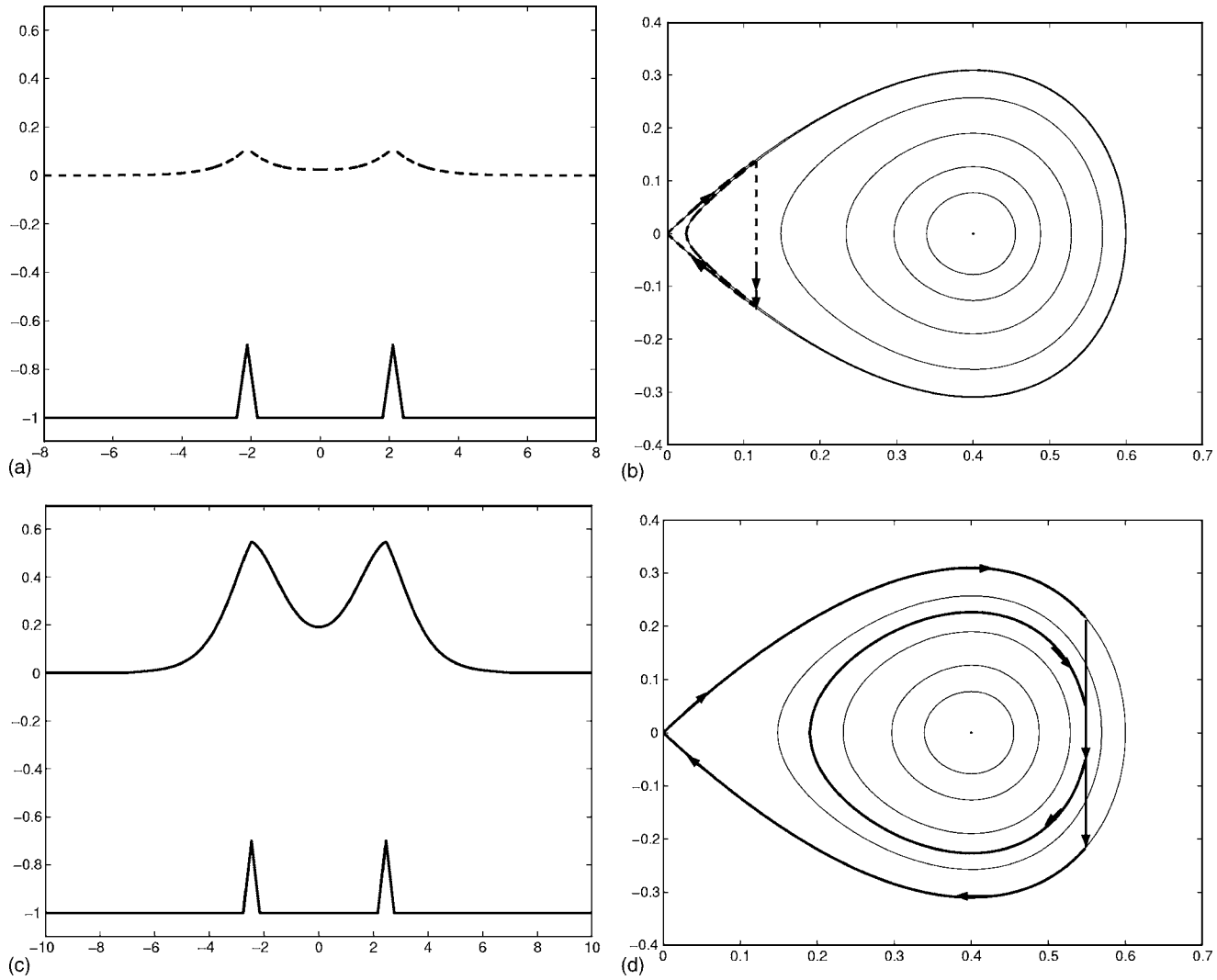

FIG. 3. Supercritical flow, $F=1.30$, $h_1=h_2=0.30$ and jumps $j_i=-3h_i^2=-0.27$. (a) Weakly nonlinear profile. The curve has maximum elevation 0.11 at x_i. The distance between the obstacles is $x_d=x_2-x_1=4.22$ and the wave amplitude at $x=0$ is 0.03. (b) Weakly nonlinear phase portrait for (a) showing $d\eta/dx$ vs η. (c) Weakly nonlinear profile. The curve has maximum elevation 0.55 at x_i. The distance between the obstacles is $x_d=x_2-x_1=4.92$ and the wave amplitude at $x=0$ is 0.19. (d) Weakly nonlinear phase portrait for (c) showing $d\eta/dx$ vs η.

$$\phi_{I+1/2}=\frac{\phi_I+\phi_{I+1}}{2},\quad I=1,\ldots,N-1, \tag{16}$$

by applying the trapezoidal rule to the integral in Eq. (9) with summation over the points ϕ_I. The symmetry of the quadrature and of the distribution of the points enables us to evaluate the Cauchy principal value as if it were an ordinary integral. The derivative in Eq. (11) is approximated at the midpoints (16) by using finite differences.

Now the dynamic boundary condition (11) can be satisfied at the midpoints (16) and this yields $N-1$ nonlinear algebraic equations. In the remainder of the paper we shall refer to this system of $N-1$ equations as the system [A].

The values of θ are known on the bottom $\psi=-1$. In order to calculate the size of the triangles we need to evaluate τ on $\psi=-1$. This is done by replacing the change of variables Eq. (8) by

$$\alpha=-e^{\pi\phi},\quad \alpha_0=e^{\pi\phi_0}. \tag{17}$$

Proceeding as in the derivation of Eq. (9), we obtain

$$\tau^B(\phi)=-\frac{1}{4}\ln\frac{(-e^{\pi\phi_1}+e^{\pi\phi})^2}{|(-e^{\pi\phi_1^{\mathrm{up}}}+e^{\pi\phi})(-e^{\pi\phi_1^{\mathrm{do}}}+e^{\pi\phi})|}-\frac{1}{4}\ln\frac{(-e^{\pi\phi_2}+e^{\pi\phi})^2}{|(-e^{\pi\phi_2^{\mathrm{up}}}+e^{\pi\phi})(-e^{\pi\phi_2^{\mathrm{do}}}+e^{\pi\phi})|}+\int_{-\infty}^{\infty}\frac{\theta(\phi_0)e^{\pi\phi_0}}{e^{\pi\phi_0}+e^{\pi\phi}}d\phi_0. \tag{18}$$

The values of y on the downstream side of the triangles can then be obtained by integrating Eq. (10)

$$y^B(\phi)=\frac{1}{\sqrt{2}}\int_{\phi}^{\phi_i^{\mathrm{do}}}e^{-\tau^B(\phi_0)}d\phi_0\quad\text{for }\phi_i<\phi<\phi_i^{\mathrm{do}},\quad i=1,2. \tag{19}$$

Equally spaced mesh points between the apexes and the downstream corners of the triangles are defined by

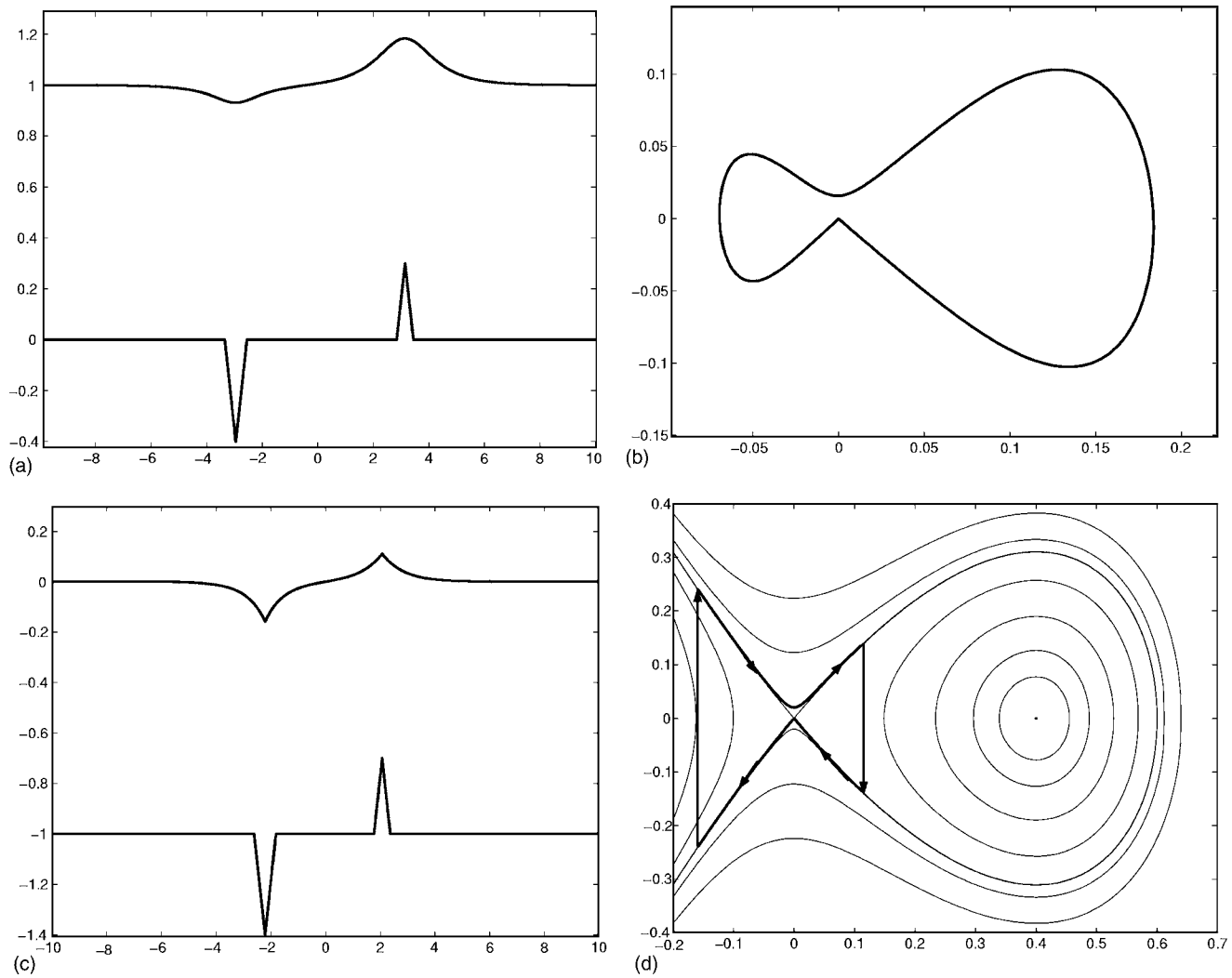

FIG. 4. Nonsymmetric supercritical flows for $F=1.30$, $h_1=-0.40$, $h_2=0.30$, $j_1=3h_1^2=0.48$, and $j_2=-3h_2^2=-0.27$. (a) Fully nonlinear free surface profile. Maximum elevation 0.18 at $x_2=3.15$ and minimum elevation -0.07 at $x_1=-2.95$, $x_d=6.10$. (b) Values of $dy/dx=\tan(\theta)$ vs $y-1=\eta$, showing the fully nonlinear phase trajectory for figure (a). (c) Weakly nonlinear profile. Maximum elevation 0.11 at $x_2=2.07$ and minimum elevation -0.16 at $x_1=-2.21$, $x_d=4.28$. (d) Weakly nonlinear phase portrait for (c) showing $d\eta/dx$ vs η.

$$\phi_{i,I}^B = \phi_i + (I-1)\frac{\phi_i^{\mathrm{do}} - \phi_i}{(N^B-1)}, \quad I=1,\ldots,N^B, \tag{20}$$

and τ^B is evaluated at the midpoints

$$\phi_{i,I+1/2}^B = \frac{\phi_{i,I}^B + \phi_{i,I+1}^B}{2}, \quad I=1,\ldots,N^B-1, \tag{21}$$

by integrating Eq. (18) numerically. Substituting these values of τ^B into Eq. (19) and integrating numerically we obtain $y^B(\phi)$. The heights of the two triangles are then given by

$$h_i = y^B(\phi_i), \quad i=1,2. \tag{22}$$

Similar equations can be derived for the values y_B on the upstream sides of the triangles by using a uniform mesh from ϕ_i^{up} to ϕ_i. Two other equations are then

$$y^B(\phi_i^{\mathrm{up}}) = 0, \quad i=1,2. \tag{23}$$

These equations ensure that the obstacles on the channel bottom are isosceles triangles with right angles at the apexes and are particularly important to impose when computing nonsymmetric free surface flows.

Values of x^B are also calculated in order to find the position of the two triangles apexes $x_i=x^B(\phi_i)$, $i=1$, 2, on the channel bottom. For given values of ϕ_i, $i=1$, 2, the distance between the two triangles is defined by

$$x_d = x_2 - x_1 = x^B(\phi_2) - x^B(\phi_1), \quad \phi_1 < \phi_2. \tag{24}$$

The system of nonlinear algebraic equations obtained after discretization is solved by Newton method. Fully nonlinear free surface profiles and fully nonlinear phase trajectories are discussed and presented in Sec. III.

As we shall see the determination of the number of independent parameters needed to obtain a unique solution is often delicate and counter intuitive. It can be found by careful numerical experimentation (fixing too many or too few parameters fails to yield convergence). An alternative approach is to perform a weakly nonlinear analysis in the phase space. This second approach has the advantage of allowing a

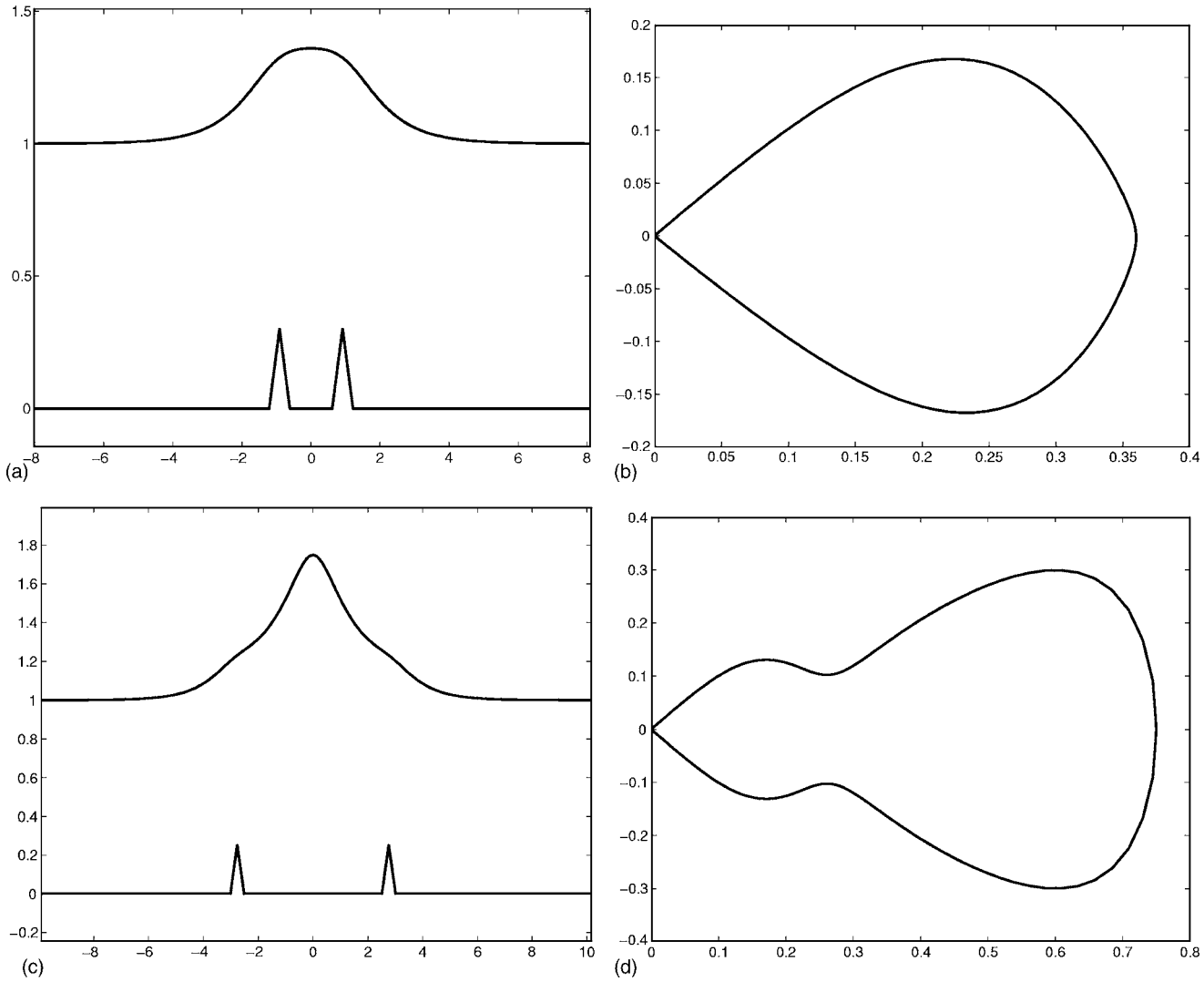

FIG. 5. Supercritical flows. (a) Fully nonlinear free surface profile for $F=1.30$, $h_1=h_2=0.30$, and $x_d=1.82$. (b) Values of $dy/dx=\tan(\theta)$ vs $y-1=\eta$, showing the fully nonlinear phase trajectory for (a). (c) Fully nonlinear free surface profile for $F=1.35$, $h_1=h_2=0.25$, and $x_d=5.52$. (d) Values of $dy/dx=\tan(\theta)$ vs $y-1=\eta$ showing the fully nonlinear phase trajectory for (c).

systematic determination of all the possible solutions (within the range of validity of the weakly nonlinear analysis). Both approches are used in this paper.

B. Weakly nonlinear theory

Shen (1995), Dias and Vanden-Broeck (2004), and others derived a forced Korteweg-de Vries equation (KdV equation) to model the flow past a disturbance in a channel. They showed that the forcing can be approximated by a Dirac delta function under certain assumptions.

Their derivation is based on long wavelength asymptotics. Thus if L denotes a typical horizontal length scale and D is the constant depth as $x^*\to-\infty$, we introduce the small parameter $\epsilon=(D/L)^2\ll 1$, the dimensionless spatial variables $(x',y')=(\epsilon^{1/2}x^*,y^*)/D$, and the free-surface elevation $e\eta'=\eta^*/D$. The equation $y^*=\sigma^*(x^*)$ describes the channel bottom in the physical coordinates. The dimensionless equation of the channel bottom is then $y'=\sigma'(x')=\epsilon^{-2}\sigma^*(x^*)/H$. In terms of these dimensionless variables the triangles heights are $h_i=h_i^*/D$ with supports $[x_i'-\epsilon^{1/2}h_i,x_i'+\epsilon^{1/2}h_i]$, $i=1,\ 2$. The Froude number F is written as $F=1+\epsilon\mu$.

Substituting expansions in powers of ϵ into the exact potential equations (rewritten in terms of the new scaled variables), the forced KdV equation is derived by equating coefficients of the powers of ϵ. The forced KdV equation (rewritten in terms of the variables $x=\epsilon^{-1/2}x'$ and $\eta=y-1=\epsilon\eta'$ used in the nonlinear computations) is

$$\eta_{xx}+\frac{9}{2}\eta^2-6(F-1)\eta=-3\sigma. \tag{25}$$

For "local" forcing, the obstacles height is comparable to the length of the base and the equation $y=\sigma(x)$ of the bottom can be approximated by the Dirac delta functions

$$\sigma(x)=Q_1\delta(x-x_1)+Q_2\delta(x-x_2). \tag{26}$$

The amplitudes Q_1 and Q_2 are determined by the areas of the triangles by integrating Eq. (26)

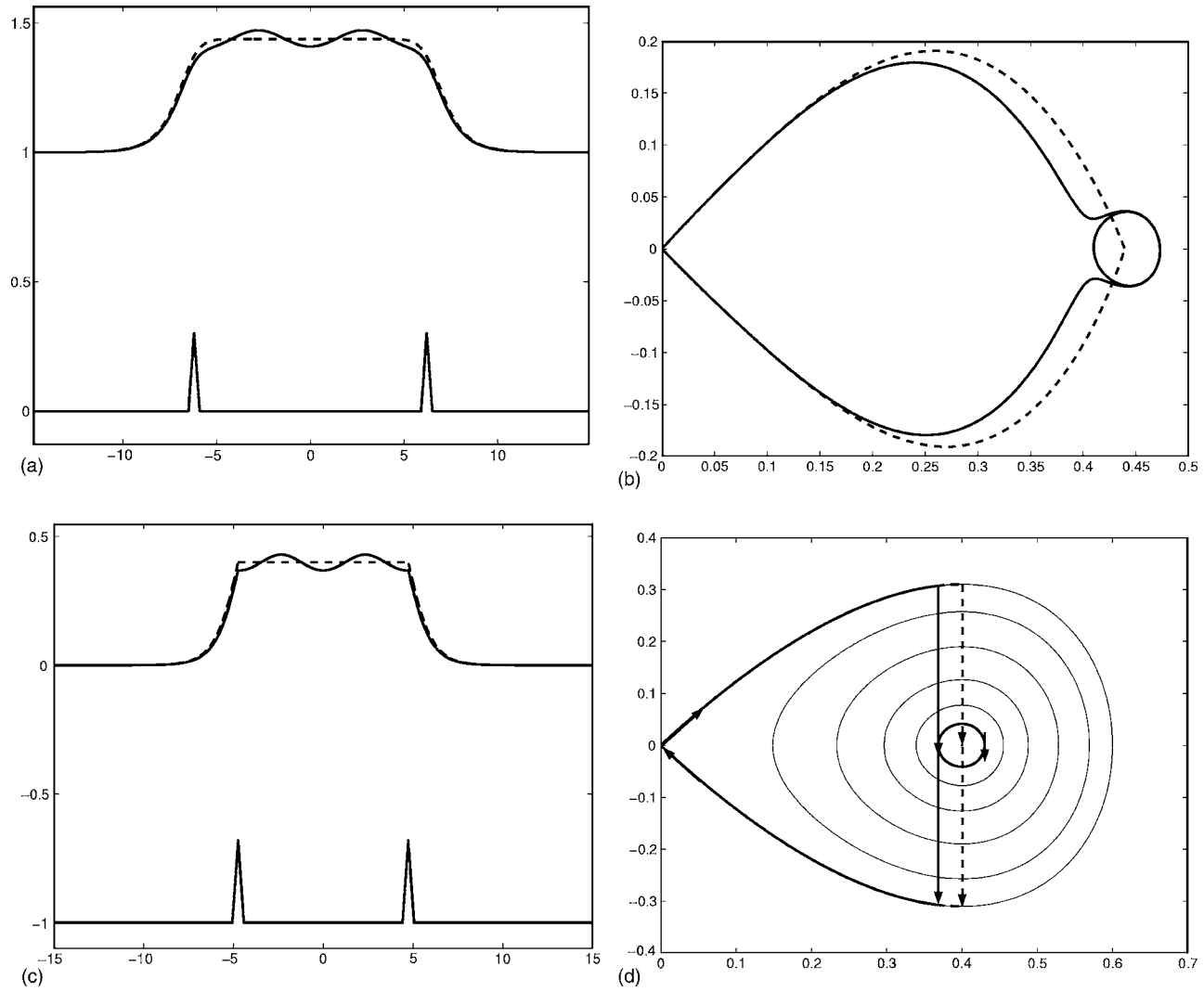

FIG. 6. Supercritical flows, for $F=1.30$. (a) Fully nonlinear free surface profiles, for $h_1=h_2=0.30$ and $x_d=12.40$. The solid curve has elevation 0.41 at $x=0$ and wave amplitude 0.06. The broken curve has elevation 0.44 at $x=0$. (b) Values of $dy/dx=\tan(\theta)$ vs $y-1=\eta$, showing the fully nonlinear phase trajectories for (a). (c) Weakly nonlinear profiles, for $h_1=h_2=0.32$, and $x_d=9.47$. The solid curve has wave amplitude 0.06. The broken curve has elevation 0.40 at $x=0$. (d) Weakly nonlinear phase portrait for (c) showing $d\eta/dx$ vs η.

$$\int_{-\infty}^{\infty}\sigma(x)dx=\int_{-\infty}^{\infty}[Q_1\delta(x-x_1)+Q_2\delta(x-x_2)]dx. \tag{27}$$

One obtains

$$Q_i=h_i^2, \quad i=1,2. \tag{28}$$

Equations (25), (26), and (28) then give

$$\eta_{xx}+\frac{9}{2}\eta^2-6(F-1)\eta=0 \quad \text{for } x\neq x_i,$$

$$\eta_x(x_i^+)-\eta_x(x_i^-)=-3Q_i=-3h_i^2 \tag{29}$$

for $i=1$, 2. We denote the jump conditions above by $j_i=-3h_i^2$. For a "dip" there is a change in sign and the jump condition is $j_i=3h^2$.

In the absence of forcing the KdV equation can be integrated as

$$\eta_x^2=6(F-1)\eta^2-3\eta^3+C, \tag{30}$$

where C is a constant of integration. Equation (30) can be used to draw phase portraits in the phase plane (η,η_x). There are two fixed points $\eta=0$ and $\eta=4/3(F-1)$.

In Sec. III weakly nonlinear phase portraits and weakly nonlinear free surface profiles are compared with the fully nonlinear results for supercritical, subcritical and critical flow.

III. RESULTS

A. Supercritical flow

For supercritical flow $U^*=U$, $H^*=H$, and $F^*=F>1$. There is in general a four parameter family of solutions. The parameters can be chosen as the distance x_d between the obstacles, the heights of the two triangles h_1, h_2, and the downstream Froude number F.

In terms of the fully nonlinear formulation, there is a total of $N+4$ unknowns ϕ_i^{up}, ϕ_i^{do}, $i=1$, 2 and θ_I, $I=1,\ldots,N$.

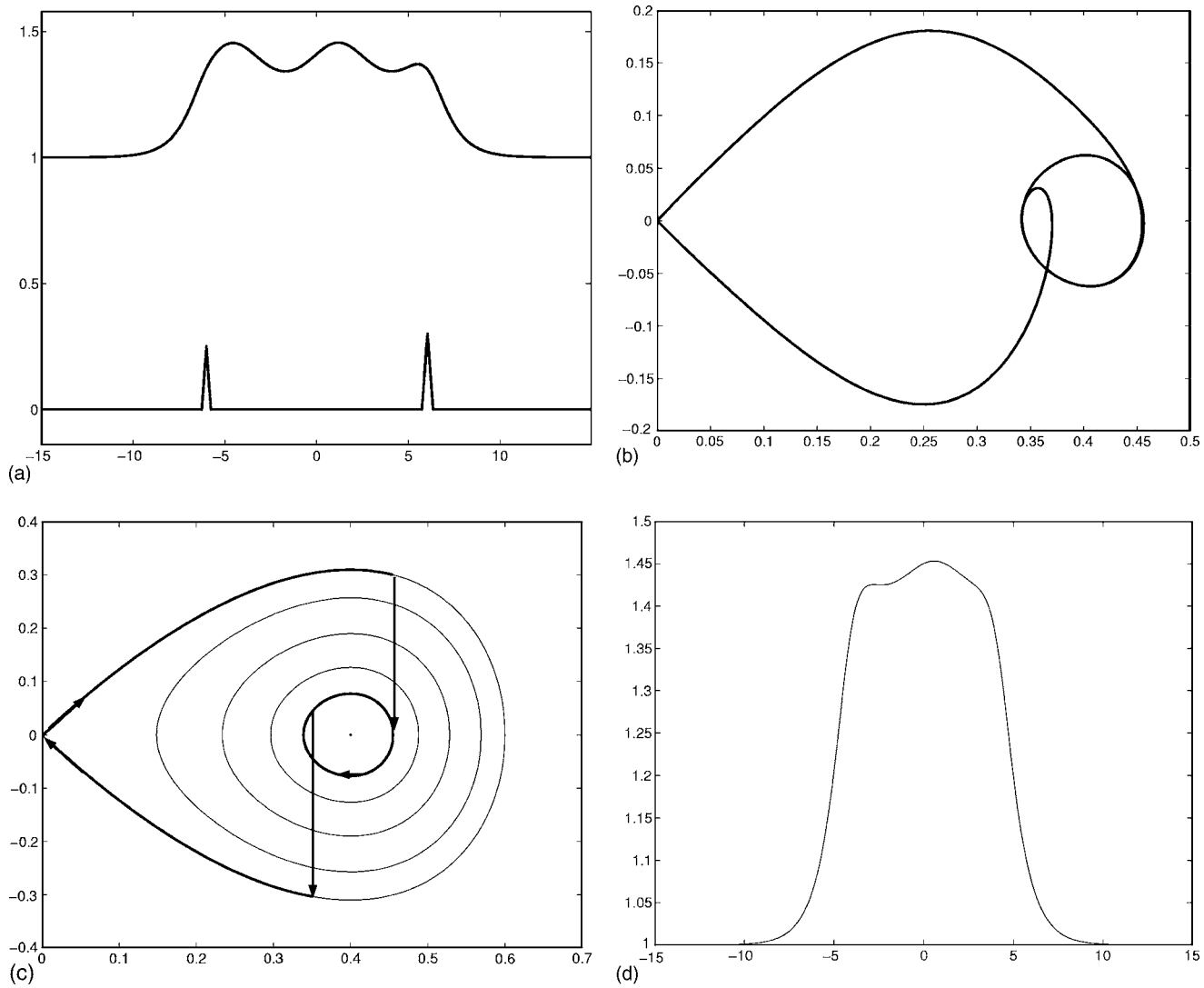

FIG. 7. Nonsymmetric supercritical flow, for $F=1.30$. (a) Fully nonlinear free surface profile, for $h_1=0.25$, $h_2=0.30$, $x_1=-6.01$, $x_2=6.05$, and $x_d=12.06$. (b) Values of $dy/dx=\tan(\theta)$ vs $y-1=\eta$, showing the fully nonlinear phase trajectories for (a). (c) Weakly nonlinear phase portrait for (a) showing $d\eta/dx$ vs η. (d) Fully nonlinear free surface profile, for $h_1=h_2=0.30$, $x_1=-4.03$, $x_2=4.05$, and $x_d=8.08$.

The $N-1$ equations obtained from [A] and Eqs. (22) and (23) yield $N+3$ nonlinear algebraic equations in terms of the $N+4$ unknowns. Forcing the free surface to be flat as $x\to-\infty$ provides the last equation $\theta_1=0$. For given values of x_d, h_1, h_2, and F, this system of equations is solved by using Newton's method.

Typical free surface profiles for $F=1.30$, $h_1=h_2=0.30$, and $x_d=6.32$ are shown in Fig. 2. These results are similar to classical supercritical flows past one obstacle. In particular these are two solutions corresponding to the same values of F, h_1, h_2, and x_d. It is interesting to note that the maximum elevation of the solid and broken curves in Fig. 2(a) do not occur at the same values of x.

The analysis in the phase plane can be described as follows. We start at the saddle point $\eta=0$ and move clockwise on the solitary wave orbit. We then have a first vertical jump j_1 onto a periodic orbit. After moving some distance on this periodic orbit we have a second vertical jump j_2 back to the solitary wave orbit and we return to the saddle point $\eta=0$. A convenient way to construct the weakly nonlinear solutions is to choose h_1, h_2, F and the value of $\eta(0)$ as the basic parameters, see Fig. 3. To compare with the fully nonlinear solutions, Fig. 2, we choose $\eta(0)=0.03$ and $\eta(0)=0.19$. This selects the inner orbit by fixing the smallest value of η for which the inner orbit intersects the η axis. The curves in Fig. 2(b) are the fully nonlinear phase trajectories for the free surface profiles in Fig. 2(a) and provide a check that the analysis in the phase plane [Figs. 3(b) and 3(d)] is qualitatively correct. The weakly nonlinear free surface profile [Fig. 3(c)] has maximum elevation $\eta=0.55$ above the two obstacles which compares well with the fully nonlinear maximum elevation $\eta=0.59$, solid curve Fig. 2(a).

We note that as $h_1\to0$ and $h_2\to0$, the solution of Fig. 3(a) approaches the saddle point of Fig. 3(b) and the flow reduces to a uniform stream. In that sense the solution of Fig. 3(a) is a perturbation of a uniform stream. Similarly as $h_1\to0$ and $h_2\to0$, the solution of Fig. 3(c) approaches the

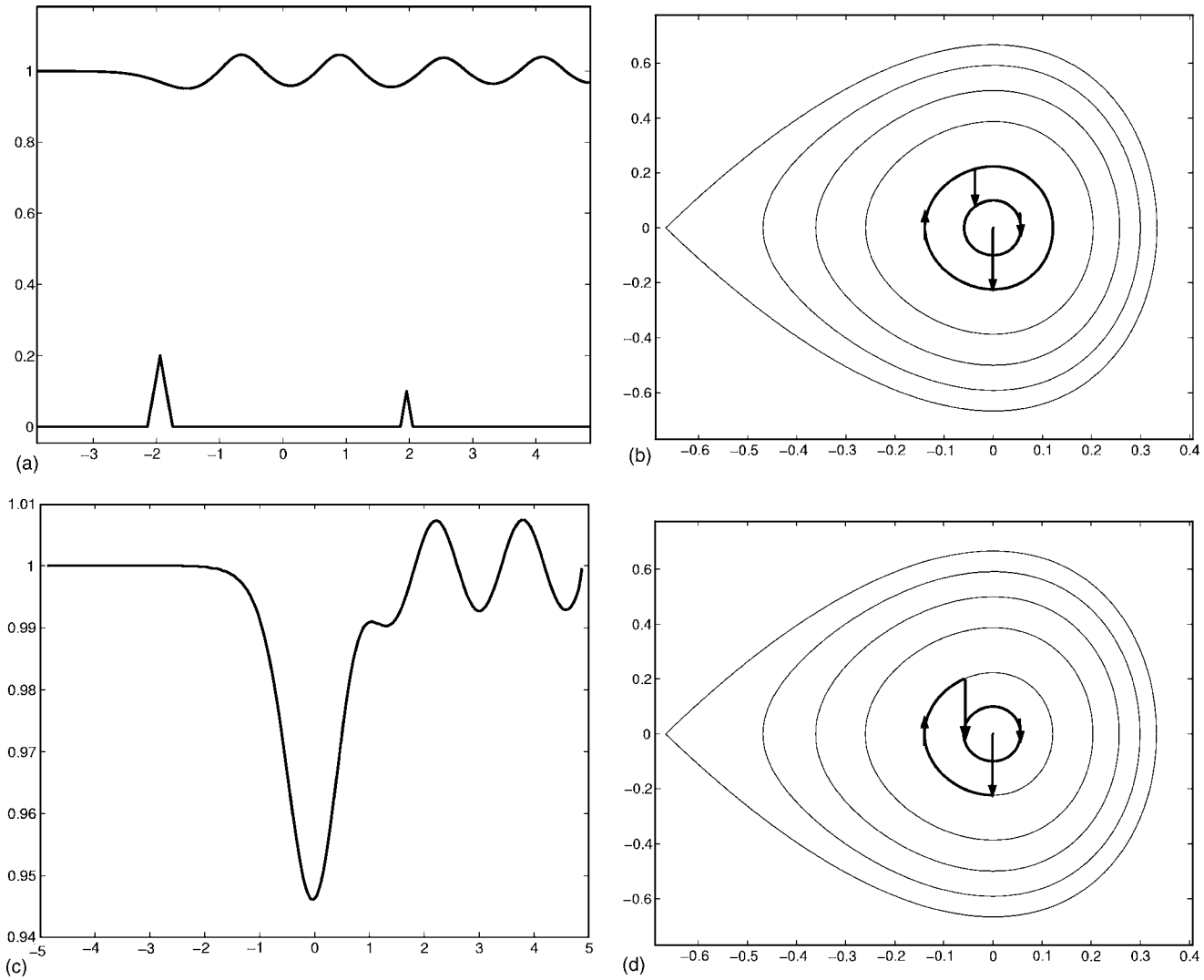

FIG. 8. Subcritical flows for $F=0.50$. (a) Fully nonlinear free surface profile, for $h_1=0.20$, $h_2=0.10$, $x_1=-1.94$, $x_2=1.95$, and $x_d=3.89$. (b) Weakly nonlinear phase portrait for (a) showing $d\eta/dx$ vs η. (c) Fully nonlinear free surface profile, for $h_1=h_2=0.20$, $x_1=-0.52$, $x_2=0.44$, and $x_d=0.96$. (d) Weakly nonlinear phase portrait for (c) showing $d\eta/dx$ vs η.

outer orbit (i.e., the solitary wave solution) in Fig. 3(d). In that sense the solution of Fig. 3(c) can be viewed as a perturbation of a solitary wave.

For given values of the Froude number and triangle heights the solutions in Fig. 2, as x_d increases, approach two solutions over a single triangle. Such solutions were calculated by Dias and Vanden-Broeck (1989). This corresponds in the phase plane of Figs. 3(b) and 3(d) to the inner orbits getting closer to the solitary wave orbit. As x_d decreases the inner orbits get closer to the center.

One way to obtain a nonsymmetric free surface profile is to choose $h_1 \neq h_2$, for given values of F and x_d. Figure 4(a) shows a fully nonlinear free surface profile for supercritical flow with $F=1.30$ past a dip, $h_1=-0.40$ and a triangle, $h_2=0.30$ on the channel bottom. It can be viewed as perturbation of a uniform stream. In the phase plane Fig. 4(d), there is now a vertical jump upwards for a dip and vertical jump downwards for a triangle. The fully nonlinear phase trajectories, Fig. 4(b), provide a check that the phase space analysis is qualitatively correct.

Two other solutions for fully nonlinear symmetric free surface profiles without a dip and their corresponding phase trajectories are shown in Fig. 5. In Fig. 5(c) the elevation of the free surface at $x=0$ is approaching a Stokes limiting configuration of 120° with a stagnation point between the two obstacles. Solutions with stagnation points cannot be accurately calculated with the uniform mesh used in this paper. However they can be computed by concentrating mesh points near the stagnation point [see, for example, Hunter and Vanden-Broeck (1983)].

Supercritical solutions with a train of waves trapped between the two obstacles were also found [see Figs. 6(a) and 7(a)]. The distance the obstacles are apart determines the number of waves trapped between the two obstacles and according to the weakly nonlinear theory this corresponds to going several times along the inner orbit.

For the symmetric flow of Fig. 6 ($h_1=h_2$), solutions can be viewed as a matching of a generalized hydraulic rise over a single triangle with a generalised hydraulic fall over a single triangle.

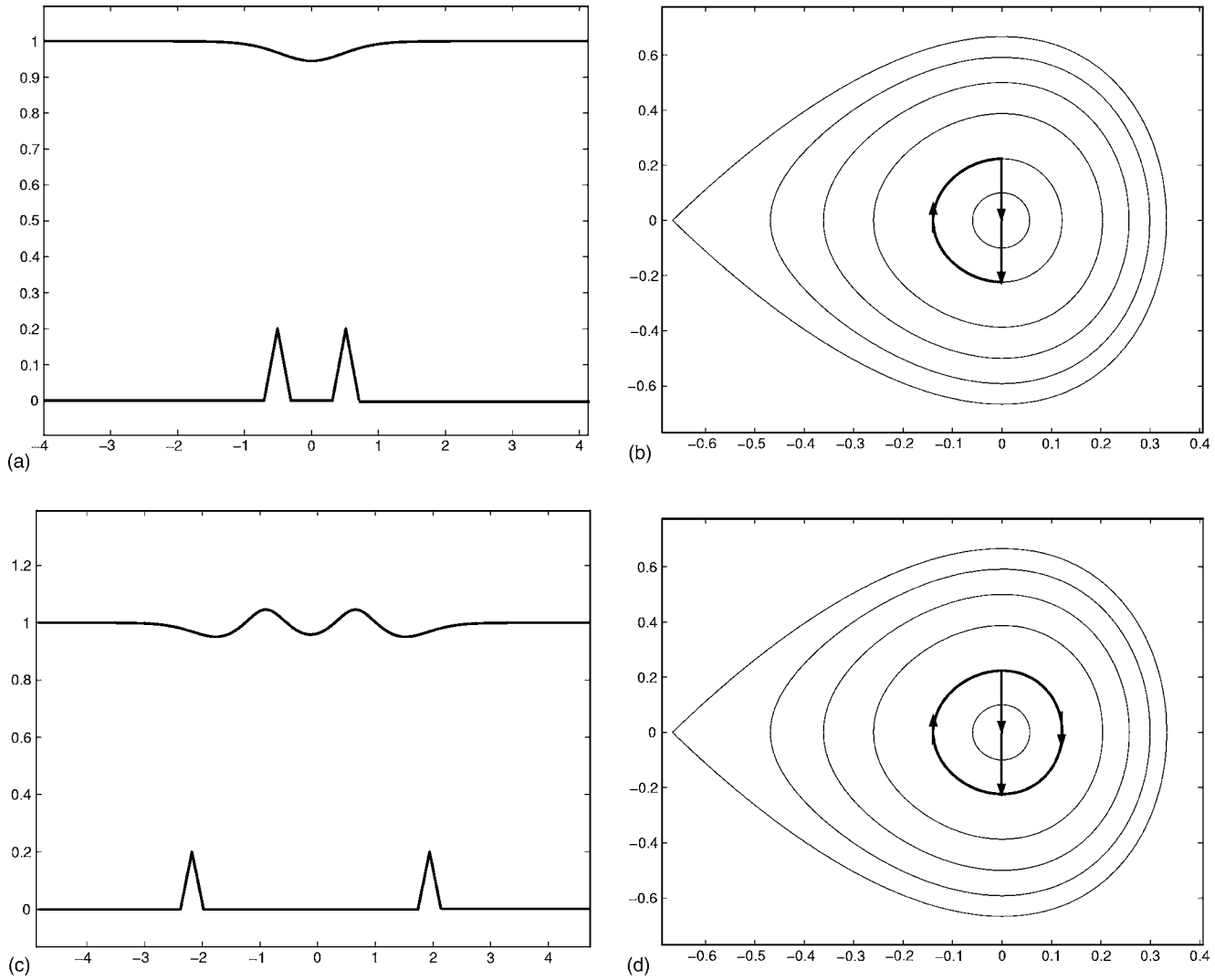

FIG. 9. Subcritical flows for $F=0.50$ and $h_1=h_2=0.20$. (a) Fully nonlinear free surface profile, for $x_2=-x_1=0.51$ and $x_d=1.02$. (b) Weakly nonlinear phase portrait for (a) showing $d\eta/dx$ vs η. (c) Fully nonlinear free surface profile, for $x_1=-2.18$, $x_2=1.94$, and $x_d=4.12$. (d) Weakly nonlinear phase portrait for (c) showing $d\eta/dx$ vs η.

These trapped waves can be eliminated midstream by satisfying

$$F^2=\frac{2y^2(0)}{1+y(0)} \tag{31}$$

on the free surface at $x=0$ [see the broken curve in Fig. 6(a)]. Equation (31) is derived by using the conservation of mass and the dynamic boundary condition (3). This waveless solution depends on one less parameter and either the Froude number or the triangles height ($h_1=h_2$) comes as part of the solution.

Using the results of weakly nonlinear theory (29) and (30), one can show that for a given value of the Froude number $F=1.30$ the triangles heights are $h_i=[(4/9)\sqrt{2}(F-1)^{3/2}]^{1/2}=0.32$ [see the broken curve in Fig. 6(c)], which compares well with fully nonlinear triangle heights $h_i=0.30$. The weakly nonlinear free surface elevation $\eta=4/3(F-1)=0.40$ also compares well with the fully nonlinear free surface elevation $\eta=y-1=0.44$ at $x=0$.

Figure 7(a) is a nonsymmetric supercritical flow with a train of waves trapped midstream for $h_1\neq h_2$ and there is no waveless solution. Another way to obtain a nonsymmetric profile is shown in Fig. 7(d), for $h_1=h_2$. Here x_d is not large enough to allow a full wavelength on the free surface between the two obstacles and solutions are non-symmetrical.

B. Subcritical flow

It is well known that subcritical potential flows are not unique, in the sense that a periodic train of waves can be added to any subcritical flow, Lamb (1945). A unique solution can be obtained by imposing the radiation condition which requires that there is no energy coming from infinity. This implies that the free surface is waveless upstream and that waves (if there are any) occur downstream. In Fig. 1(a) (which assumes a uniform stream as $x\to\infty$), the flow then needs to be from right to left (i.e., the direction of the flow needs to be reversed).

In general a four parameter family of solutions was found for subcritical flow past two triangles. These parameters can be chosen as the downstream Froude number F, the triangles heights, h_1, h_2, and the distance x_d between the two obstacles.

Figure 8(a) is a typical fully nonlinear free surface profile for $F=0.50$, $h_1=0.20$, $h_2=0.10$, and $x_d=3.83$. In this figure (as well as in all the others in this section), we have reversed the flow so that all the profiles in the paper correspond to flow from left to right. There are two trains of periodic waves differing in amplitude on the free surface. One is trapped between the two triangles and the other is downstream of the two triangles.

The analysis in the phase plane can be described as follows. We start at the center point $\eta=0$ and have a first vertical jump j_1 onto an inner periodic orbit. After moving clockwise some distance on this periodic orbit we have a second vertical jump j_2 in general onto another periodic, see Fig. 8(b). We have not compared qualitatively the weakly nonlinear phase portrait with the corresponding fully nonlinear phase trajectories because the value $F=0.50$ is not close to one.

For triangles of the same height $h_1=h_2=0.20$ and given value of the Froude number $F=0.50$, there are in general two trains of periodic waves on the free surface downstream of the obstructions, similar to those already discussed in Fig. 8(a).

The train of trapped waves can be eliminated by decreasing x_d. An example for $x_d=0.96$, $F=0.50$, and $h_i=0.20$, is shown in Fig. 8(c). Analysis of the phase space is illustrated in Fig. 8(d).

Similarly for triangles with $h_1=h_2$, the downstream train of waves can be eliminated by adjusting x_d, see Fig. 9(c). Such solutions for two distributions of pressure with compact support were calculated before by Vanden-Broeck (2002). This solution depends on one less parameter and x_d comes as part of the solution. If in addition the triangles are close enough together then both trains of waves can be eliminated as shown in Fig. 9(a).

Figures 8(b), 8(d), 9(b), and 9(d) show that according to the weakly nonlinear theory, h_1 can be different from h_2 in the flows of Fig. 8 but that $h_1=h_2$ in flows of Fig. 9.

C. Hydraulic jumps

In general there is a four parameter family of solutions with two trains of periodic waves on the upstream free surface. This flow is illustrated in Fig. 1. The independent parameters can be chosen as the downstream Froude number F, the heights of the two triangles h_i, and the distance x_d between the two obstacles.

If there are waves far upstream on the free surface the radiation condition is violated, as energy is coming in from $x=-\infty$. As shown in Dias and Vanden-Broeck (2004), these waves can be eliminated far upstream thus making the solution physically realistic. It is shown in Fig. 10(a).

These solutions only depend on two parameters for example h_1 and h_2. The downstream Froude number F and distance x_d between the triangles are allowed to come as part of the solution. The equation

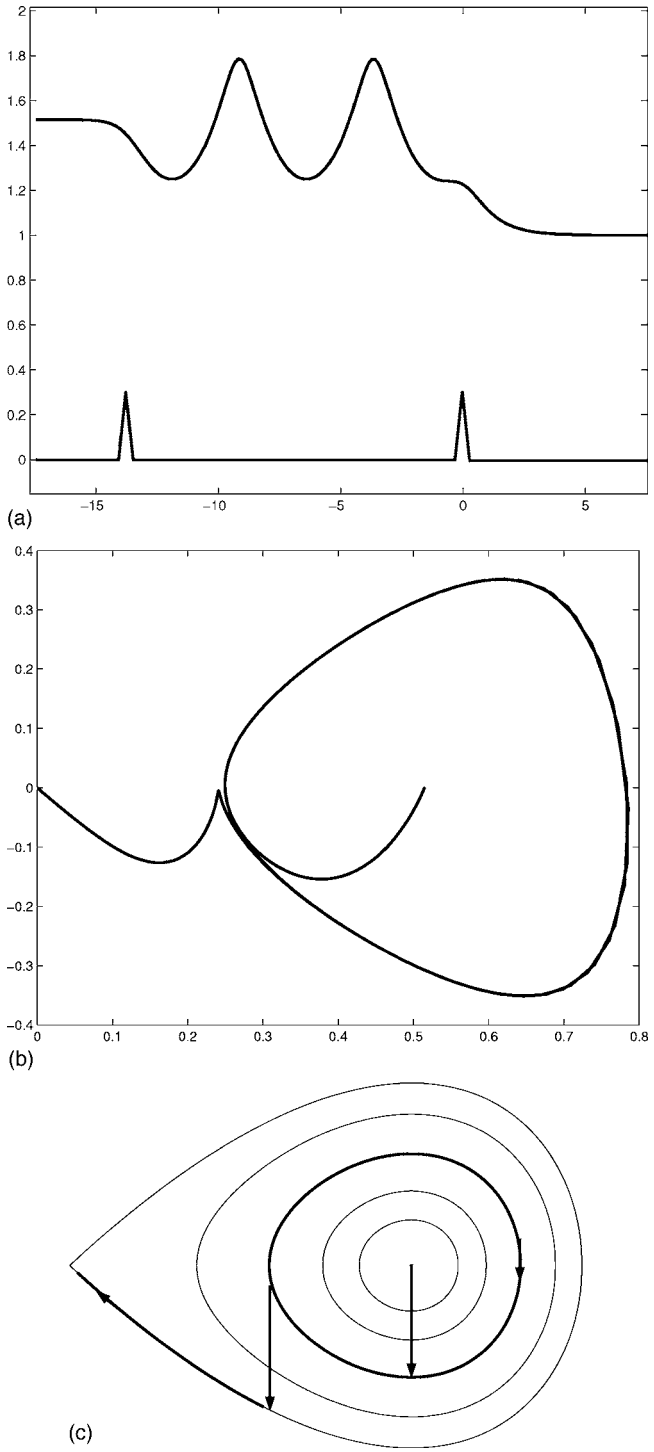

FIG. 10. Hydraulic jumps for $F=1.35$ and $h_1=h_2=0.30$. (a) Fully nonlinear free surface profile, for $x_1=-13.75$, $x_2=0.0$, and $x_d=13.75$. (b) Values of $dy/dx=\tan(\theta)$ vs $y-1=\eta$, showing the fully nonlinear phase trajectories for (a). (c) Weakly nonlinear phase portrait for (a) showing $d\eta/dx$ vs η.

$$F^2=\frac{2y^2(-\infty)}{1+y(-\infty)} \tag{32}$$

has to be satisfied on the upstream free surface as $x\to-\infty$. Equation (32) is derived by using the conservation of mass and the dynamic boundary condition (3). A qualitative weakly nonlinear analysis of the phase space is illustrated in

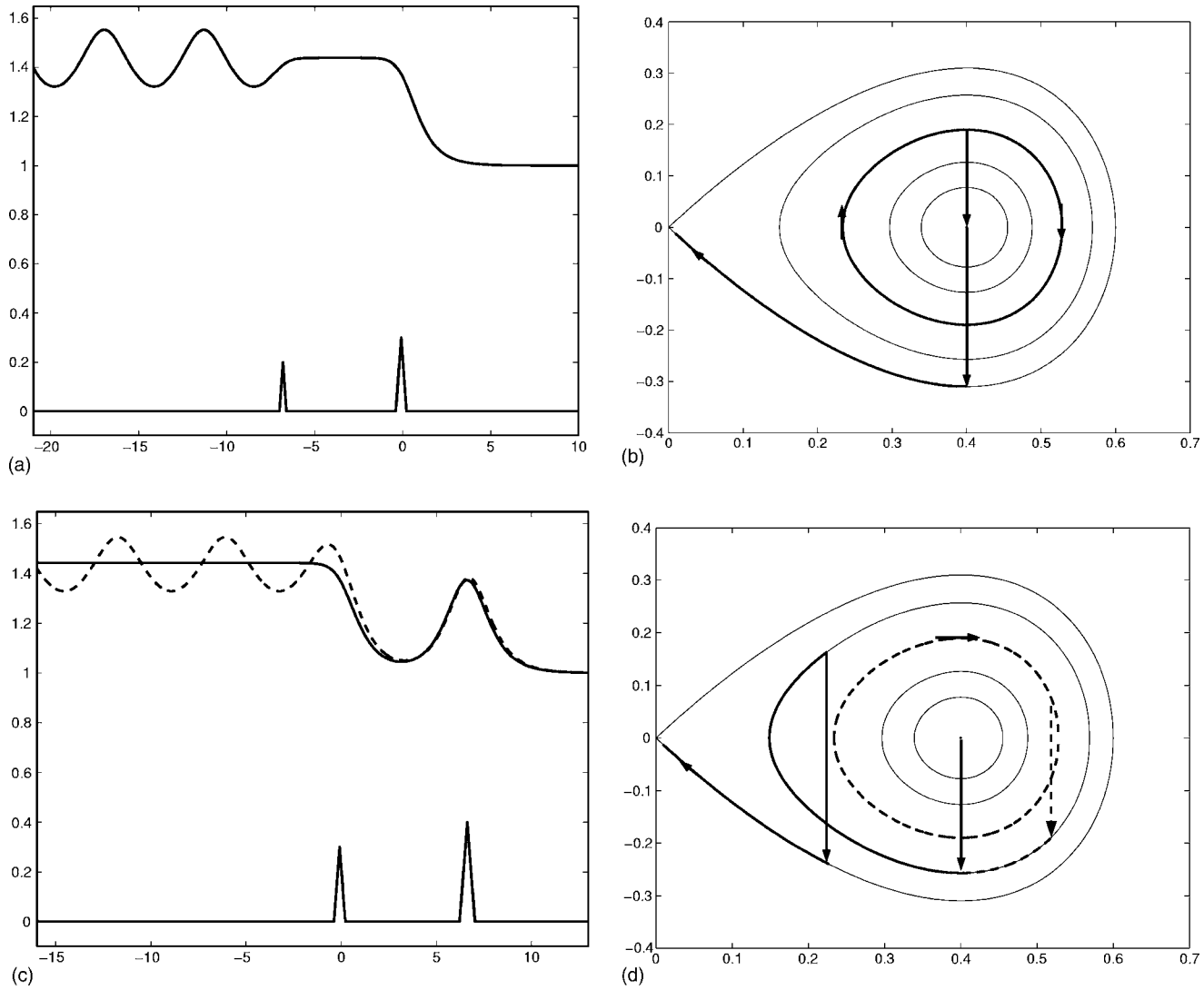

FIG. 11. Hydraulic jumps for $F=1.30$.(a) Fully nonlinear free surface profile, for $h_1=0.20$, $h_2=0.30$, $x_1=-6.73$, $x_2=0.0$, and $x_d=6.73$. (b) Weakly nonlinear phase portrait for (a) showing $d\eta/dx$ vs η. (c) Fully nonlinear free surface profiles, for $h_1=0.30$, $h_2=0.40$, $x_1=0.0$, $x_2=6.70$, and $x_d=6.70$. (d) Weakly nonlinear phase portraits for (c) showing $d\eta/dx$ vs η.

Fig. 10(c) and the fully nonlinear trajectory shown in Fig. 10(b) confirms that it is correct.

Figure 11(a) is a new type of solution where the waves have been eliminated between the two obstacles. There is a train of waves far upstream. These solutions do not satisfy the radiation condition as $x\to-\infty$, but could be made physically realistic by the introduction of a third disturbance far upstream. The triangle heights h_i were chosen as the independent parameters. The downstream Froude number F and distance x_d between the two obstacles were allowed to come as part of the solution. Analysis in the phase plane is illustrated in Fig. 11(b).

Finally, in Fig. 11(c) another new type of fully nonlinear solutions is shown. As before there is a four parameter family of solutions with waves on the upstream free surface. The waveless solution depends on one less parameter. Analysis of these two types of solutions in the phase plane is shown in Fig. 11(d).

IV. CONCLUSIONS

Supercritical, subcritical, and critical flows over two obstacles on a channel bottom were considered. Fully nonlinear solutions were calculated by a boundary integral equation method and weakly nonlinear solutions were derived. Classical solutions were recovered and new solutions such as those in Fig. 11 were found. No attempt was made to justify rigorously the results from the weakly nonlinear analysis. The problem is to find all flows of sufficiently small amplitude. Without the obstacles, the stationary problem can be treated as an evolution equation in the unbounded space variable. In the presence of the obstacles, the problem becomes "nonautonomous" in the sense that the isotropy in the unbounded variable is broken by the obstacles. The analysis of Mielke (1986) could be used to obtain rigorous results.

ACKNOWLEDGMENTS

This research was partially supported by Alliance (the Franco-British Joint Research Programme of the British Council, with Project No. 05697WF), EPSRC, and the National Science Foundation.

[1]Baines, P. G. (1995). *Topographic Effects in Stratified Flows* (Cambridge University Press, New York), p. 482.
[2]Dias, F., and Bridges, T. J. (2005). "The numerical computation of freely propagating time-dependent irrotational water waves," Fluid Dyn. Res. (to be published).
[3]Dias, F., and Vanden-Broeck, J.-M. (1989). "Open channel flows with submerged obstructions," J. Fluid Mech. **206**, 155–170.
[4]Dias, F., and Vanden-Broeck, J.-M. (2002). "Generalised critical free-surface flows," J. Eng. Math. **42**, 291–301.
[5]Dias, F., and Vanden-Broeck, J.-M. (2004). "Trapped waves between submerged obstacles," J. Fluid Mech. **509**, 93–102.
[6]Forbes, L.-K. (1981). "On the resistance of a submerged semi-elliptical body," J. Eng. Math. **15**, 287–298.
[7]Forbes, L.-K. (1988). "Critical free-surface flow over a semi-circular obstruction," J. Eng. Math. **22**, 3–13.
[8]Grimshaw, R. H. J., and Smyth, N. (1986). "Resonant flow of a stratified fluid over topography," J. Fluid Mech. **169**, 429–464.
[9]Hunter, J. K., and Vanden-Broeck, J.-M. (1983). "Accurate computations for steep solitary waves," J. Fluid Mech. **136**, 63–71.
[10]Lamb, H. (1945). *Hydrodynamics*, 6th ed., Chap 6, 411 pp.
[11]Mielke, A. (1986). "Steady flows of inviscid fluids underlocalized perturbations," J. Diff. Eqns. **65**, 89–116.
[12]Pratt, L. J. (1984). "On nonlinear flow with multiple obstructions," J. Atmos. Sci. **41**, 1214–1225.
[13]Shen, S. S-P. (1995). "On the accuracy of the stationary forced Korteweg-de Vries equation as a model equation for flows over a bump," Q. Appl. Math. **53**, 701–719.
[14]Vanden-Broeck, J.-M. (2002). "Waves trapped under a moving pressure distribution," *IUTAM Symposium on Diffraction and Scattering in Fluid Mechanics and Elasticity* (Kluwer Academic, Dordrecht), Vol. 41, pp. 61–68.
[15]Watters, G. Z., and Street, R. L. (1964). "Two-dimensional flow over sills in open channels," J. Hydr. Div., Proc. ASCE **90**, 107–140.